PERGAMON

Acta mater. 48 (2000) 1131–1140

Acta MATERIALIA

www.elsevier.com/locate/actamat

THE GENERATION OF INTERGRANULAR STRAINS IN 309H STAINLESS STEEL UNDER UNIAXIAL LOADING

J. W. L. PANG[1]†, T. M. HOLDEN[2]‡, J. S. WRIGHT[3] and T. E. MASON[1]§

[1]Department of Physics, University of Toronto, 60 St. George Street, Toronto, Ontario, Canada M5S 1A7, [2]Neutron Program for Materials Research, Steacie Institute for Molecular Sciences, National Research Council, Chalk River, Ontario, Canada K0J 1J0 and [3]ISIS Facility, Rutherford Appleton Laboratory, Chilton, Didcot, Oxfordshire OX11 0QX, UK

(Received 2 July 1999; accepted 12 October 1999)

Abstract—The generation of intergranular strains in 309H austenitic steel has been measured *in situ* up to 13.0% deformation by neutron diffraction. Experimental data have been obtained in the directions parallel and perpendicular to the tensile axis. Large tensile strains are observed for the (002) reflection along the tensile axis while the other reflections show relatively small intergranular effects. Both texture and residual strain states of the as-received and deformed samples have also been measured. The number of grains with [111] parallel to the tensile axis increases from ×2 to ×4 random texture and is coupled with a depletion of [220] grains in the same direction. The *in situ* experiments have been simulated with the EPSC model of Turner and Tomé. The model tends to overestimate the intergranular strains in the directions perpendicular to the tensile axis. © *2000 Acta Metallurgica Inc. Published by Elsevier Science Ltd. All rights reserved.*

Keywords: Stress–strain relationship measurements; Austenitic steel; Neutron scattering

1. INTRODUCTION

When a polycrystalline sample is loaded beyond its macroscopic yield point, the strain response of each individual grain depends on its orientation with respect to the loading axis because of anisotropy in the elastic and plastic deformation of the material at the single crystal level. These differences in the strain response of the grains create incompatibilities on the length scale of the grains in a single-phase polycrystal. Stress and strain continuities between grains can be maintained by the introduction of strain within the grains that varies with grain orientation.

If the applied loading is such that all the grains deform elastically, the strains within the grains will disappear when the load is removed because of the reversible nature of elastic deformation. As the applied loading increases, plastic deformation preferentially begins in grains that are favourably orientated to have their slip systems activated, whereas other grains remain in the elastic regime. Just as for inhomogeneous elastic deformation, elastic strains will be developed in the grains to maintain continuities among the neighbouring grains. The elastic strains that develop in the grains to accommodate inhomogeneous plastic deformation during the macroscopic elasto-plastic transition are termed the intergranular strains. These vary with grain orientation and are dependent on the magnitude of the elastic and plastic deformations, and the texture of the sample. The grain size is usually many orders of magnitude smaller than the sample dimension. Within a small macroscopic volume within a sample, the summation of the intergranular stresses, weighted by the texture, over the grains must balance. Since plastic deformation is largely irreversible, the intergranular strains remain as type-II strains in the grains when the load is removed.

Neutron diffraction is a powerful tool for measuring residual strains non-destructively since neutrons can penetrate deeply into the bulk of samples. For example, practical measurements can be made through 200 mm of Al and 20 mm of Fe. The principle of neutron diffraction strain measurements is based on Bragg's law:

$$\lambda = 2d_{hkl} \sin \theta_{hkl} \tag{1}$$

† To whom all correspondence should be addressed. Present address: Manchester Materials Science Centre, Grosvenor Street, Manchester M1 7HS, UK.

‡ Present address: Northern Stress Technologies, 5 Spring Street, Deep River, Ontario, Canada K1J 1P0.

§ Present address: Spallation Neutron Source, Oak Ridge National Laboratory, TN 37831-8218, USA.

1359-6454/00/$20.00 © 2000 Acta Metallurgica Inc. Published by Elsevier Science Ltd. All rights reserved.
PII: S1359-6454(99)00382-1

where λ is the neutron wavelength, d_{hkl} is the lattice spacing of planes with plane normals $[hkl]$ and $2\theta_{hkl}$ is the corresponding angle of diffraction. d_{hkl} is determined by measuring either $2\theta_{hkl}$ with fixed λ, or the wavelength distribution of the scattered neutrons at a fixed diffraction angle. Each peak gives the average lattice spacing of the set of grains that have a particular crystallographic direction $[hkl]$ along the direction which bisects the incident and scattered beams. Lattice strains are determined from the shifts in lattice spacing with the following equation:

$$\varepsilon_{hkl} = \frac{d_{hkl} - d^0_{hkl}}{d^0_{hkl}} \tag{2}$$

where d^0_{hkl} is the stress-free lattice spacing. The lattice strain measured consists of the type-I strains, ε^{I} in addition to the average intergranular strain $\varepsilon^{\mathrm{int}}_{hkl}$ of the particular set of grains characterized by $[hkl]$. The magnitude of the intergranular strain provides profound insight into the micromechanisms of the deformation of polycrystalline materials.

The measurements of the evolution of intergranular strains in polycrystalline materials at the grain level by neutron diffraction began about 10 years ago. Information on the intergranular strains in various materials generated during the elasto-plastic transition is now available. This includes a series of h.c.p. Zr-based alloys [1–3], f.c.c. Ni-based alloys [4–6], pure polycrystalline Cu and Al [7], Al7050 [8], a b.c.c. ferritic steel 350WT [9] and an austenitic stainless steel [10]. In this paper, experiments carried out to characterize the development of intergranular strains in the austenitic 309H stainless steel under uniaxial tension are presented. An experiment on an austenitic steel has been performed by Clausen *et al.* [10] in which the evolution of intergranular strain *in situ* up to 2% plastic strain was measured in directions both parallel and perpendicular to the tensile axis. In this experiment the *in situ* measurements in the directions parallel and perpendicular to the load axis were made to much higher strains, up to 8 and 13% deformation, than previously [10]. In addition to the *in situ* measurements in the sample principal directions, measurements were also made over a wide angular range before and after the loading test, to find the angular variation of residual intergranular strains in the sample. Simulations of the experimental results based on the elasto-plastic self-consistent (EPSC) model of Turner and Tomé [11, 12] were carried out.

2. EXPERIMENTS

The experiments on steel tensile samples described below were divided into three parts. First, the texture and the residual strain in the as-received state were measured. The samples were then subjected to uniaxial loading and the lattice strain response was measured *in situ* as a function of applied stress. *In situ* experiments were carried out both at the ISIS spallation source at the Rutherford Appleton Laboratory, UK and the NRU reactor at the Chalk River Laboratories, Canada. Finally the texture and the residual strains in the deformed samples were determined.

2.1. Samples

A 309H stainless steel rolled plate was supplied by Rockwell International (Milton, Ontario, Canada). 309SS is a f.c.c. austenitic steel with alloying elements of 23 wt% Cr, 14 wt% Ni, 2 wt% Mn, 1 wt% Si, 0.2 wt% C and less than 0.1 wt% of other elements. The tabulated values of the yield point and Young's modulus of the bulk are 275 MPa and 200 GPa [13]. The steel is elastically anisotropic and the diffraction elastic constants of the hardest and the softest directions differ by about 60%. The steel is also plastically anisotropic and deforms by slip along the $\langle 10\bar{1} \rangle$ directions in the $\{111\}$ planes.

The sample, designated S_I, prepared for the *in situ* experiment carried out at ISIS, was cylindrical with a diameter of 4.535 ± 0.002 mm. The rolling direction (RD) of the plate was parallel to the tensile axis. The normal direction (ND) and the transverse direction (TD) of the plate were perpendicular to the stress axis. Three dogbone samples prepared for the *in situ* experiments at Chalk River were $6.98 \times 7.00\ \mathrm{mm}^2$ in cross-section and are designated S_{C1}, S_{C2}, S_{C3}. The RD of the plate lay along the tensile axis and the ND and the TD lay in the transverse plane as shown in Fig. 1.

2.2. Characterization of the received sample

The experiments to determine the texture and residual strains of small coupons of the as-received sample were made on the E3 spectrometer at the NRU reactor. A neutron wavelength of 1.1123 Å, obtained by reflection from the (117) planes of a Ge monochromator, was used. The divergence of the

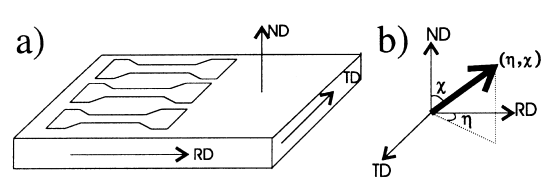

Fig. 1. (a) The sample orientation with respect to the rolling direction (RD), the transverse direction (TD) and the normal direction (ND) of the rolled plate. (b) The sample spherical coordinate system. χ is the angle between the plate normal direction and the angular orientation of the measurement. η is the angle which the RD makes with the projection of the angular orientation of the measurement in the RD–TD plane.

incident and the scattered beam was 0.3°. The coupon was centred on an Eulerian cradle that in turn was centred on the spectrometer table. The spherical coordinate system (η, χ) used to describe the angular orientation of the sample is illustrated in Fig. 1. Pole figures for the (111), (002) and (220) reflections were obtained by measuring the Bragg peak intensity over a hemisphere on a $5° \times 5°$ grid. The orientation distribution function (ODF) of the sample was calculated by least squares fitting data from the three pole figures simultaneously [14]. The angular variations of residual strain for the (111), (002), (220) and (113) reflections were measured over a $15° \times 15°$ grid of one quadrant of the pole figure with the same experimental set-up as in the texture measurements.

2.3. *In situ intergranular strain measurements*

2.3.1. Fixed wavelength diffraction. The experiments were carried out on the N5 spectrometer at Chalk River using neutrons of wavelength 1.4783 Å generated by reflection from the (115) planes of a Si monochromator. The collimation of the beam before and after the sample was 0.2°. Uniaxial tension was provided by a universal testing machine (UTM) from Applied Test Systems (Butler, PA, USA), mounted on the spectrometer. The total deformation, ε_{tot}, was measured with an extensometer mounted on the sample.

The lattice strain response, ε_{lat}, in the sample parallel to the tensile axis was measured for reflections (111), (002), (220) and (113) at multiple stress levels. Each peak necessarily includes contributions from all the crystal orientations with lattice plane normal [*hkl*] lying along the scattering vector. Measurements were also made in the other two principal directions transverse to the stress axis, corresponding to the TD and ND of the rolled plate, with separate samples designated S_{C1}, S_{C2} and S_{C3}, for the respective directions.

The applied stress, σ_{app}, was increased incrementally to a maximum and then decreased to zero. The peak stress for the first cycle was 300 MPa which is above the 0.2% offset yield point of the bulk as-received material, σ_y, and was increased for each successive cycle. The total plastic deformations for the samples S_{C1}, S_{C2} and S_{C3} were 7.2, 13.0 and 12.5%. Many measurements were made in the elastic region, below 80% of σ_y, during the initial stage of the first cycle. The slope and the intercept obtained from the linear fit to the linear elastic response give, respectively, a proportional constant, E_{hkl}, between the applied stress and the linear elastic strain response and a reference lattice spacing, d^{ref}_{hkl} for each reflection (*hkl*), at zero stress.

As the applied stress increases beyond the yield point, intergranular strains, ε^{int}_{hkl}, generated because of inhomogeneous plastic deformation, contribute to the total lattice strain at any given stress, in addition to the linear elastic strain, as follows:

$$\varepsilon^{lat}_{hkl} = \varepsilon^{int}_{hkl} + \frac{\sigma_{app}}{E_{hkl}} \tag{3}$$

where σ_{app}/E_{hkl} is the linear elastic strain corresponding to σ_{app}. The first indications of intergranular strains are the deviations of ε_{lat} from the initial linear elastic response. In general, the linear elastic strains are much greater than the intergranular strains. The quoted applied stresses, σ_{app}, are true stresses.

Note that the reference spacings, d^{ref}_{hkl}, are the lattice spacings at the start of the tensile test and are not necessarily stress-free. The advantage of using these reference spacings is that the intergranular strains correspond to the intergranular effects caused by the applied loading only and are independent of previous history.

2.3.2. Time-of-flight diffraction. A tensile test experiment was also made by diffraction using a white neutron beam on the ENGIN time-of-flight spectrometer at the ISIS spallation source. The strain responses both parallel (RD of the rolled plate) and perpendicular (TD of the rolled plate) to the stress axis were measured simultaneously using counters at $\pm 90°$. The placement of the sample with respect to the neutron beam is shown in Fig. 2. The stress rig used to provide uniaxial tension was provided by Imperial College. Unlike a reactor source, the simultaneous availability of a range of wavelengths in the beam, 0.5–3 Å, means data are available from a range of d-spacings simultaneously. Figure 3 shows a typical spectrum measured in a single run. The diffraction elastic constants, the reference lattice spacings and the extraction of ε^{int}_{hkl} from the lattice strain measurements were determined as described earlier.

For time-of-flight diffraction, the line shape of a diffracted peak is a complicated function of time

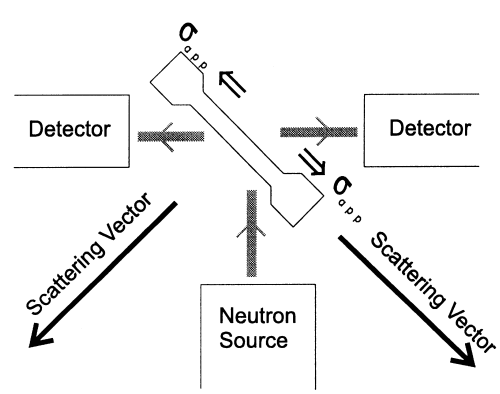

Fig. 2. Orientation of the sample with respect to the neutron beam for measurements on ENGIN at ISIS. Measurements parallel and perpendicular to the stress axis are made at the same time.

[15] rather than a simple Gaussian for a conventional angular diffractometer. The peak shape involves a sharp leading edge and a lagging exponential tail convoluted with a Gaussian function. In general, Rietveld analysis [15] is used to analyse the time-of-flight powder diffraction pattern in which all the Bragg peaks are fitted simultaneously. Since intergranular effects are not considered in the Rietveld routine, it was not used to analyse the present experiment. Instead, fitting routines for individual Bragg peaks were developed to determine the lattice spacings.

2.4. Residual strain and texture of the deformed samples

The (111), (002) and (220) pole figures of the deformed sample S_{C2} with 13% deformation were measured as described in Section 2.2. The residual strain state of the 8% deformed sample, S_I, was determined from the (111), (002), (220) and (113) reflections over a quadrant of orientations on a $5^\circ \times 5^\circ$ grid, and from the (331), (420) and (422) reflections on a $15^\circ \times 15^\circ$ grid with a neutron wavelength of 1.1008 Å reflected from the (117) planes of Si.

The net residual stress averaged over all grain orientations in the small coupon must be zero. Thus, by measuring the lattice spacings of a number of reflections in many sample directions, the corresponding average lattice parameter should approach the stress-free value, a^0. In principle, the value of a^0 determined from the deformed sample should be equal to that of the undeformed sample and this was found to be the case to within the quoted experimental errors which represent the r.m.s. deviation from the mean.

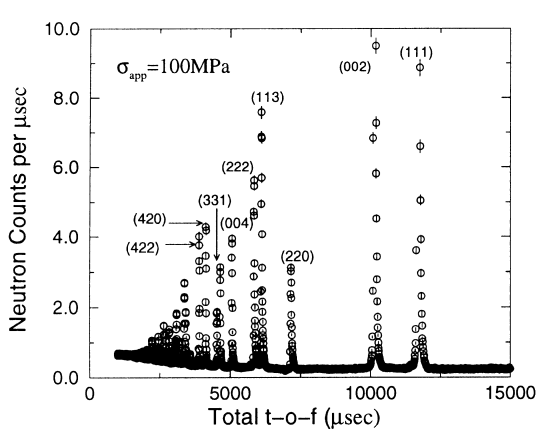

Fig. 3. Indexed time-of-flight spectrum obtained with the ENGIN at an applied stress of 100 MPa.

3. EXPERIMENTAL RESULTS

3.1. Texture and residual strain of the received sample

The (111), (002) and (220) pole figures of the as-received sample are shown in Fig. 4(a) which displays mild rolling texture. The initial strain state of the sample was measured for these three reflections plus the (113) reflection at 15° intervals over a quadrant of 4π. The average lattice parameter for all measurements, i.e. the global stress-free a^0, was found to be $3.5967 \pm 0.0001\,\mathring{A}$. The residual strains were found to be small, and to lie within a band of $\pm 2 \times 10^{-4}$ for all reflections.

3.2. In situ tensile test experiments

3.2.1. Time-of-flight diffraction. The lattice strain responses parallel and perpendicular to the stress axis were measured simultaneously as the stress was increased incrementally to 458 MPa corresponding to a plastic deformation of 8.0%. The flow curve of the sample is shown in Fig. 5. Young's modulus for the sample and the 0.2% offset yield point were measured to be 196 ± 6 GPa and the 0.2% offset yield point was ~ 265 MPa.

Only the strains measured with the (002) planes show an appreciable deviation from linearity in the diagram of lattice strain vs applied stress and the results are shown as crosses in Fig. 6. The responses for the other planes are linear to within $\pm 2 \times 10^{-4}$. The precision of the response for each individual strain value, as determined from the peak fitting routines, is smaller than $\pm 0.5 \times 10^{-4}$. However, the scatter along the initial elastic locus suggests that the real uncertainty is on the order of $\pm 1 \times 10^{-4}$. For the strain response perpendicular to the stress

Table 1. Initial linear responses of 309SS for applied stresses less than 80% of the macroscopic yield stress in the rolling direction (RD), parallel to the tensile axis, and in the transverse (TD) and the normal (ND) directions, perpendicular to the tensile axis, for the reflections (111), (002), (220) and (113). The experimental results are compared with the EPSC model including the rolling texture, the Kröner model with no texture. All values are in the units of GPa

	EPSC	Kröner	Expt
RD			
(111)	236	242	239 ± 8
(002)	147	152	129 ± 7
(220)	215	211	220 ± 9
(113)	178	184	167 ± 9
TD			
(111)	−871	−1052	-905 ± 56
(002)	−472	−461	-425 ± 41
(220)	−668	−796	-578 ± 48
(113)	−578	−626	-594 ± 65
ND			
(111)	−927	−1052	-1005 ± 53
(002)	−449	−461	-398 ± 49
(220)	−808	−796	-770 ± 61
(113)	−589	−626	-597 ± 72
Bulk	194	196	196 ± 6

axis, no reflection exhibits an intergranular strain of magnitude greater than 2×10^{-4}.

3.2.2. Fixed wavelength diffraction. In situ experiments were repeated at the NRU reactor to obtain the unloading behaviour as well as the strain response along the ND of the plate. The average stress–strain curve of the three samples, S_{C1}, S_{C2} and S_{C3}, is shown together with the stress–strain curve of sample S_I (Fig. 5). The diffraction elastic constants, obtained from the linear fit of the initial elastic response, are shown in Table 1. The single crystal elastic constants of stainless steel of chemical composition $Fe_{0.68}Cr_{0.18}Ni_{0.14}$ [16], $c_{11} = 198.0$ GPa, $c_{12} = 125.0$ GPa, $c_{44} = 122.0$ GPa, were used to calculate the diffraction elastic constants with the Kröner model [17]. The calculated bulk elastic constant agrees with the experimental result within error.

The lattice strain response also confirmed the experiment done with the ISIS spallation source. Apart from the (002) planes that develop a large tensile intergranular strain along the stress axis, the strain response of the other planes for all three principal directions is of the order of the experimental uncertainty. Measurements for the (002) reflection parallel to the stress axis are plotted together with the ISIS results in Fig. 6. With the aid of equation (3), the intergranular strains for the (002)

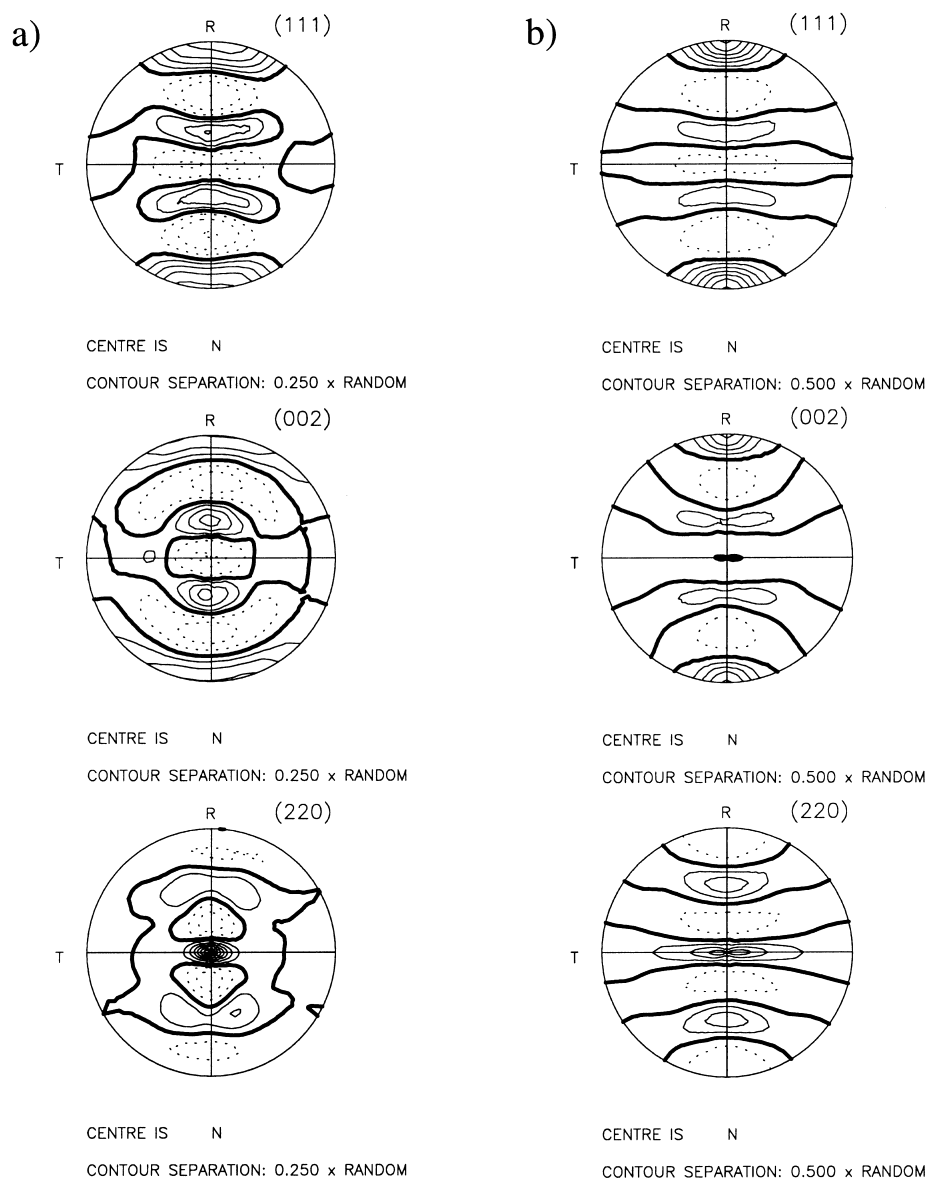

Fig. 4. (111), (002) and (220) pole figures of a coupon of (a) the as-prepared sample and (b) the sample deformed to 13%. The contour corresponding to $1.0 \times$ Random is designated by a heavy solid line. Contours above and below $1.0 \times$ Random are decorated by solid and dotted lines, respectively.

reflection can be separated from the linear elastic behaviour and are plotted in Fig. 7. The uncertainties of the intergranular strains are on the order of $\pm 2 \times 10^{-4}$.

Initially there are no intergranular effects, the response is linearly elastic and $\varepsilon_{int} = 0$. Above 200 MPa, which is still 60 MPa below the 0.2% yield point of the bulk material, a tensile intergranular strain was observed which increases gradually with σ_{app}. If the unloading was completely elastic, the intergranular strain would stay unchanged from the value at the maximum stress and the unloading curve would be vertical. However, in fact, the unloading was not linear. The magnitudes of the tensile intergranular residual strains were generally smaller than the intergranular strains at the maximum stress of each cycle and the difference became larger as the plastic deformation increased. It was also found that the successive loading path does not follow the unloading path of its preceding cycle. Instead, a clockwise loop is formed which enlarges as deformation increases. The final residual strain for the (002) planes is 8×10^{-4}, corresponding to a total plastic deformation of 7.2%.

The initial, nominally linear elastic responses from Fig. 7 appear to be different after the second and third cycles. The difference is ascribed to a redistribution of residual stresses on loading and unloading and not to a change in the intrinsic elastic behaviour of the material. Other reflections must also show similar departures from the intrinsic behaviour, but these lie within the uncertainties of the experimental results for our stainless steel material. The (002) behaviour stands out because of the low intrinsic elastic stiffness in this direction as well as the low multiplicity of (002) planes. In principle, there should also be deviations in the initial slopes of the as-received material from intrinsic elastic behaviour since the material had been plastically deformed by rolling. However, as was indicated above, the residual strains due to the rolling process were small, even for the (002) direction, and hence any deviations were masked by the experimental uncertainty.

3.2.3. Diffracted peak intensity changes during tensile testing. The integrated intensities of the peaks change as grain reorientations take place during plastic deformation. Figure 8 shows the relative changes of the intensities for the (111), (002), (220) and (113) peaks parallel to the tensile axis measured with the sample S_{C1}. The (111) peak shows an increase in intensity of about 30% whereas the intensity of the (220) peak drops by about 60%. Similar observations in the changes in intensity were found with sample S_I. The experimental results agree qualitatively with the predicted grain rotations of a f.c.c. alloy [18]. When the direction of the applied stress is near the [110] direction in a crystallite, the dislocations move and the crystal tends to rotate so that the [111] direction becomes parallel to the load axis.

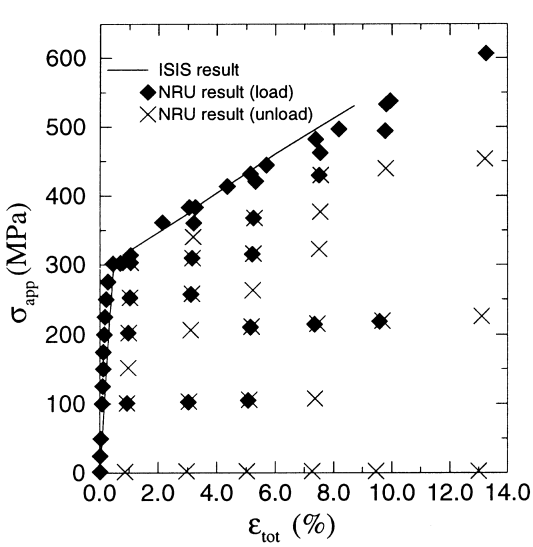

Fig. 5. Stress–strain curve for the 309H stainless steel samples measured at ISIS and NRU.

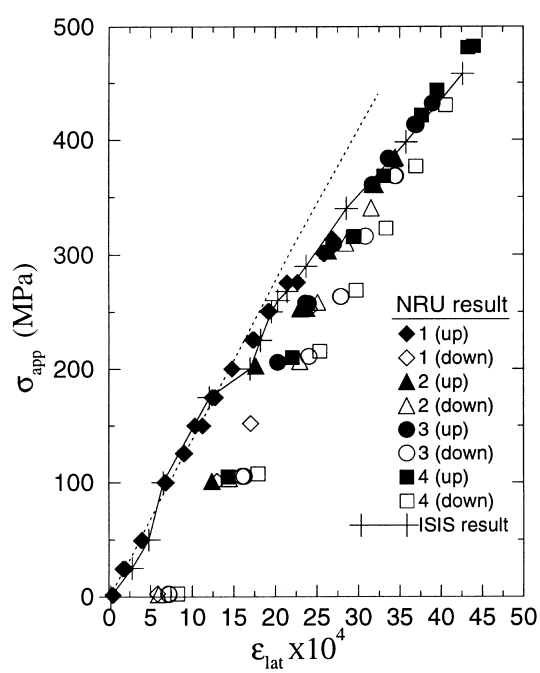

Fig. 6. The lattice strain response for the (002) reflection parallel to the stress axis in the rolling direction of the original plate. Data obtained from the ISIS spallation source and the NRU reactor are both displayed. The dashed line is the linear elastic response calculated with the average diffraction elastic constant determined from the two separate experiments.

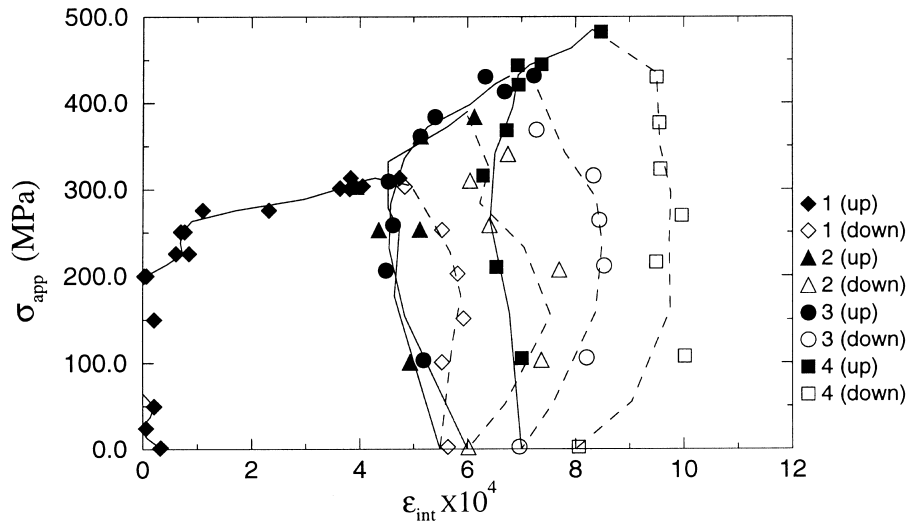

Fig. 7. The intergranular strain response for the (002) reflection parallel to the stress axis (and in the rolling direction of the original plate). The solid and dashed lines are guides for the loading and unloading paths of each cycle, respectively.

3.3. Texture and residual strain state of a deformed sample

The pole figures for the (111), (002) and (220) reflections of the deformed sample S_{TD} (13% deformation) are shown in Fig. 4(b). The texture of the deformed sample is very different from the texture of the sample before deformation [see Fig. 4(a)] indicating that grain reorientation has taken place during the tensile test as also shown in Section 3.2.3. The number of grains with direction [111] parallel to the load axis (RD of the rolled plate) increases from ×2 to ×4 random texture. The number of [002] grains has also been increased from ×1.6 to ×2 random. The increase in [111] and [002] grains along the tensile axis is accompanied by a depletion of [220] grains in this direction.

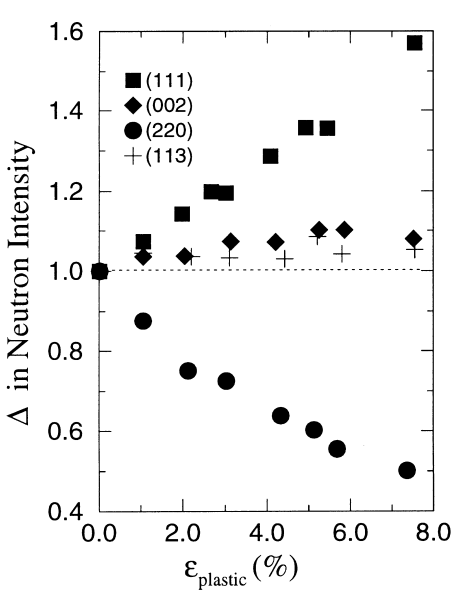

Fig. 8. Relative change of the scattered neutron intensity along the tensile axis for reflections (111), (002), (220) and (113) as a function of plastic deformation.

The residual strain state of the sample S_I (8% deformation) was measured to examine whether there are balancing strains in directions other than the principal directions. The average lattice parameter, averaged over all sample directions and four crystallographic reflections is 3.5966 ± 0.0001 Å which agrees with the global stress-free a^0 measured with the as-prepared sample, to within experimental error. Residual strain pole figures for reflections (111), (002), (331) and (422) are shown in Fig. 9. Except for the (002) reflection, all reflections display small compressive strains with magnitudes smaller than -3×10^{-4} in nearly all sample directions. An axisymmetric pattern about the applied stress direction RD is found for the (002) pole figure. The magnitudes of the residual strains along the principal directions agree with the measurements for the 7.2% deformed sample in the unloaded state in the *in situ* experiment performed at the NRU reactor.

4. SIMULATIONS OF THE INTERGRANULAR STRAINS

4.1. Theory

The elastic stresses and strains which develop in the grains making up a polycrystalline aggregate to compensate the incompatibilities due to elastic and plastic anisotropy were studied by Hill [19, 20] and Hutchinson [21]. Their analyses are implemented in the elasto-plastic self-consistent (EPSC) model which is a numerical code developed by Turner and Tomé [11, 12].

In the EPSC model, each grain is considered as

an ellipsoidal inclusion within a homogeneous effective medium that has the average behaviour of all the grains. The orientation of each grain is specified by three Euler angles (θ, ϕ, ω) which relate the crystallographic axes of the grain to the sample coordinate system. The volume fraction of each orientation is taken into account by assigning a weight factor $w(\theta, \phi, \omega)$ to each set of Euler angles and these are matched to the strong texture. Based on the self-consistent scheme, the constraints implemented in the model are that the average of the stress rates and strain rates, $\{\dot{\sigma}\}$ and $\{\dot{\varepsilon}\}$, of all the grains are equal to the overall stress and strain rates, $\dot{\Sigma}$ and $\dot{E}$, of the aggregate.

While the stress remains below yield, results from the EPSC model are essentially identical to the Kröner model. However, within the EPSC model, the matrix is permitted to be anisotropic and there are no constraints on the sample texture. During plastic deformation, the type and number of slip systems that are activated in each grain are calculated by the code. Hardening parameters that are matched to the stress–strain curve strongly affect the residual strains. The modifications of the interaction tensors that relate the stresses and strains of the grains with those of the homogeneous effective medium, through the elastic constants and hardening parameters, are constantly updated as deformation proceeds. By specifying either $\dot{\Sigma}$ and $\dot{E}$ as the boundary condition, the stress and strain of each grain and the overall responses can be determined self-consistently based on the relationships among $\dot{\sigma}$, $\dot{\varepsilon}$, $\dot{\Sigma}$ and $\dot{E}$ developed in Hill's scheme [19, 21].

4.2. Simulations of the experimental results by the EPSC model

The orientation distribution function of the sample prior to the tensile test was integrated over a $10^\circ \times 10^\circ \times 10^\circ$ Euler space to generate a discrete set of volume-weighted grains (2014) as a representation of the sample texture. The single crystal elastic constants of stainless steel of chemical composition $Fe_{0.68}Cr_{0.18}Ni_{0.14}$ [16] were used. The 12 f.c.c. slip systems are those of the type $\{111\} \times \langle 10\bar{1} \rangle$. Self-hardening was assumed and the onset of each slip system was assumed to be independent of the others.

The experimental flow curve was matched closely

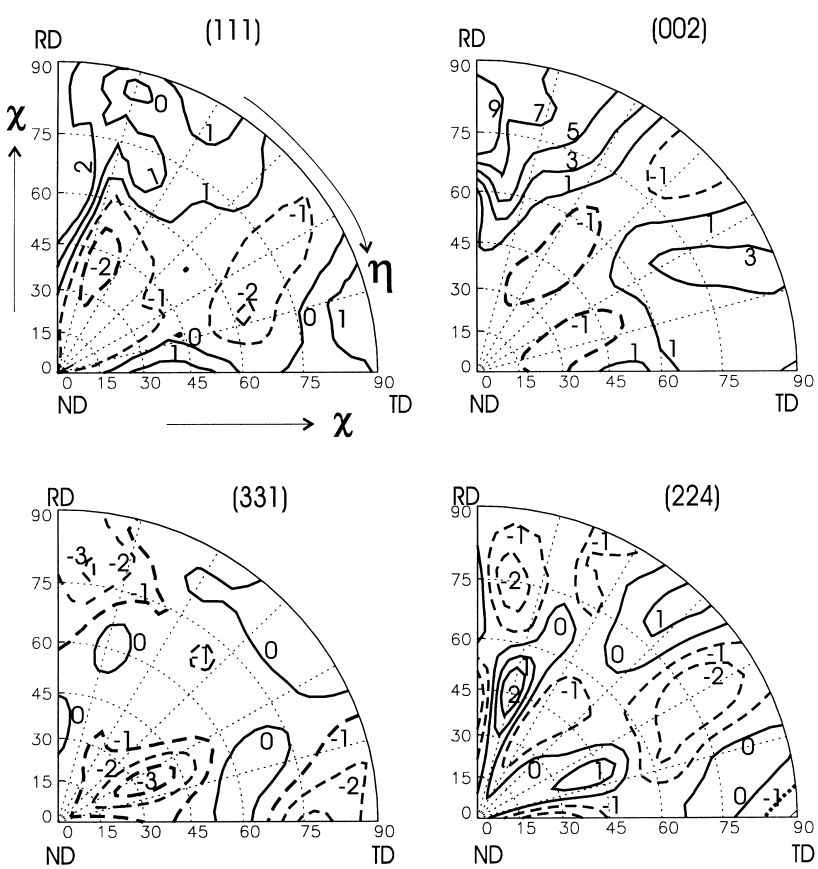

Fig. 9. Residual strain state of sample S_I deformed to 8% as measured with the (111), (002), (331) and (224) planes. Compressive strains are indicated by dashed contour lines and tensile strains are indicated by solid contour lines. All strains are in the units of 10^{-4}.

by choosing the critical resolved shear stress to be 95 MPa and the hardening parameter to be 2.8 GPa that matched the slope of the plastic region of the stress–strain curve. The initial slopes in the linear elastic region determined from the two sets of experiments are listed together with the EPSC model and the Kröner model calculations in Table 1. Calculated diffraction elastic constants and the experimental values agree to within experimental errors in general. It is interesting to note that the slopes of the (220) response, for the two transverse directions: TD and ND differ by 30%. The difference is likely to be due to the strong concentration of [220] poles in the transverse plane. The texture sensitive EPSC model calculation captures this behaviour but not the Kröner model in which random texture is assumed.

The calculated lattice strains for the (111), (002), (220) and (113) reflections in sample S_I after 8% deformation are tabulated together with the experimental results in Table 2. The calculated lattice strain response beyond the macroscopic yield point differs from that observed experimentally. The EPSC model predicts large tensile intergranular strains in excess of 6×10^{-4} after 8% deformation for the (002) reflections in all the three principal directions: RD, ND and TD. In contrast, the only significant intergranular strains observed in the experiment are those near the stress axis (RD) for the (002) reflection as in Fig. 9. Since the simulated elastic response is in good agreement with the experiment, it is believed that the causes of the strain discrepancies are the inadequate descriptions of the hardening of the slip systems or inadequate understanding of the modes of plastic deformation in 309SS. Homotectic hardening was tested (the activation of a slip system has the same hardening effects on all the other slip systems) but the results are similar to those obtained with self-hardening except that the largest magnitude of the strains dropped to 6×10^{-4}. It is worth noting that in the case of Monel-400 [5] and Inconel-600 [6], the calculated (002) intergranular strains perpendicular to the stress axis were always greater (typically a factor of two) than the experimental strains, which were however notably tensile. In 309SS the transverse strains as measured, are definitely zero unlike Monel and Inconel.

Table 2. Lattice strain responses of sample S_I for the reflections (111), (002), (220) and (113) after 8% deformation in the rolling direction (RD), parallel to the tensile axis, and in the transverse (TD) and the normal (ND) directions, perpendicular to the tensile axis. The experimental results are compared with the EPSC model including the rolling texture. All values are in units of 10^{-4}

	EPSC	Expt
RD		
(111)	1	-2 ± 1
(002)	8	7.7 ± 0.8
(220)	−4	-1.3 ± 2.5
(113)	−1	1.2 ± 0.3
TD		
(111)	−1	0.2 ± 0.9
(002)	6	0.7 ± 0.6
(220)	−2	-4 ± 0.9
(113)	1	1.1 ± 0.3
ND		
(111)	−2	-1 ± 1
(002)	9	0.7 ± 0.5
(220)	−2	-4.1 ± 0.3
(113)	3	-0.4 ± 0.3

5. DISCUSSIONS AND CONCLUSIONS

Large intergranular strains are only observed in grains which have [002] directions within 30° of the tensile axis where 309H stainless steel is subjected to uniaxial stress. The present results confirm measurements on a similar austenitic stainless steel [10] deformed to 2% in uniaxial tension, where the intergranular strains in grains with [002] directions transverse to the stress direction were also close to zero. This result contrasts with the behaviour in Monel-400 [5] and Inconel-600 [6], which have similar elastic and plastic anisotropy as 309H stainless steel, but show tensile intergranular strains in grains with [002] directions aligned perpendicular to the stress axis. The intergranular strains measured with the aid of reflections other than (002) do show systematic variations with respect to the applied stress axis, but they are not more than about two times their assigned uncertainties. It is to be expected that compressive stresses in grains with other than [002] orientations balance the tensile [002] oriented grains and this appears to happen as seen in the (331) and (224) strain pole figures, Fig. 9, near the rolling direction.

The differences in slopes of the (220) response in the two transverse directions perpendicular to the tensile axis indicate the effect of texture on elastic anisotropy. This is not unexpected because the strain developed in each grain orientation due to elastic anisotropy depends on the strain response of the other orientations in its surroundings.

It is observed that the intergranular strain increment is largest for the first loading–unloading cycle and is less for the subsequent cycles. This may be explained by the fact that, as the applied stress increases, the slip systems of the grains which are difficult to activate because of their orientations with respect to the load axis, become active. The onset of plastic deformation in more grains reduces the intergranular effects in subsequent loadings since the incompatibilities among grains are then accommodated by means of slip instead of the generation of elastic strains. Another feature observed in the tensile test is the open loop formed in the stress–strain response following the unloading path of one cycle and the successive loading path of the next cycle for (002) orientations. These hysteresis loops may possibly be explained by the presence of defects such as vacancies that form obstacles for the motion of dislocations taking place in slip. The ac-

cumulation of dislocations around the defects may modify the strain response of the grains when the samples are reloaded after unloading.

The validity of the elasto-plastic self-consistent (EPSC) model has also been tested against experiment. For the simulations of the initial linear elastic response, the only parameters required are the single crystal elastic constants and the orientation distribution of the sample. The predicted behaviour is in good agreement with experiments. The ability of the EPSC model to take into account the effect of texture is an improvement over the Kröner model in predicting the elastic behaviour of polycrystalline materials. The intergranular strains, generated because of anisotropic plastic and elastic deformation, simulated with the EPSC model are not in very good agreement with experiment.

A major difficulty with the model is the definition of hardening for each slip system. The type of hardening used in the present simulations is linear hardening which assumes the critical resolved shear stress, τ_c, of a slip system increases at a constant rate as plastic deformation increases. The advantage of a simple linear hardening model is that the number of parameters needed for the calculations is small—one for each type of slip system. However, this assumption may, in fact, be too simple to describe the actual situation. Clausen and Lorentzen [7] and Weng [22] have independently proposed non-linear hardening functions in which the hardening rate decreases as plastic deformation increases.

Another deficiency of the EPSC model is that it fails to simulate the hysteresis loops observed in Fig. 7 for the (002) strains. The model predicts that the lattice strains for all reflections should follow a linear unloading path whose slope is parallel to the initial slope of the stress–strain curve. Figure 7 shows that there is a redistribution of strain among the grains which is a function of the magnitude of the applied stress. The hysteresis loops have been observed in the majority of materials studied to date.

It is important to note that twinning is another mode of the plastic deformation mode which can take place in austenitic steel because of the low stacking fault energy [23]. The shear strains introduced by twinning will modify the lattice strain responses but were not considered in the EPSC model. At present, the EPSC code does not account for twinning but the inclusion of this feature is under development [24].

Acknowledgements—We wish to thank J. H. Fox and L. E. MacEwen for experimental assistance and sample preparation. We are also grateful to Professor G. Webster and Dr A. Ezeilo of Imperial College, London for providing us the stress rig at ISIS. This work was supported by the Natural Sciences and Engineering Research Council (NSERC) and the Ontario Centre for Materials Research (OCMR). T. E. Mason thanks the Alfred P. Sloan Jr Foundation for support.

REFERENCES

1. MacEwen, S. R., Tomé, C. and Faber Jr, J., *Acta metall.*, 1989, **37**, 979.
2. MacEwen, S. R., Christodoulou, N. and Salinas-Rodriguez, A., *Metall. Trans.*, 1990, **21A**, 1083.
3. Pang, J. W. L., Holden, T. M. and Mason, T. E., *J. Strain Analysis*, 1999, **33**, 373.
4. Holden, T. M., Clarke, A. P. and Holt, R. A., *J. Neutron Res.*, 1997, **5**, 241.
5. Holden, T. M., Clarke, A. P. and Holt, R. A., *Metall. Trans.*, 1997, **28A**, 2565.
6. Holden, T. M., Holt, R. A. and Clarke, A. P., *Mater. Sci. Engng*, 1998, **A246**, 180.
7. Clausen, B. and Lorentzen, T., *Metall. Trans.*, 1997, **28A**, 2537.
8. Pang, J. W. L., Holden, T. M. and Mason, T. E., *Acta mater.*, 1998, **46**, 1503.
9. Pang, J. W. L., Holden, T. M., Mason, T. E. and Panza-Giosa, R., *Physica B*, 1998, **241–243**, 1267.
10. Clausen, B., Lorentzen, T., Bourke, M. A. M. and Daymond, M. R., *Mater. Sci. Engng*, 1999, **A259**, 17.
11. Turner, P. A. and Tomé, C. N., *Acta metall.*, 1994, **42**, 4043.
12. Turner, P. A., Christodoulou, N. and Tomé, C. N., *Int. J. Plasticity*, 1995, **11**, 251.
13. Brandes, E. A. and Brook, G. B. (ed.), *Smithells Metals Reference Book*, 7th edn. Butterworth Heinemann, London, 1992.
14. Root, J. H. and Holden, T. M., Programs to determine the crystalline orientation distribution function from diffraction intensity pole figures (ANDI-29) of Atomic Energy of Canada Limited, 1990.
15. Windsor, C. G., *Pulsed Neutron Scattering*. Taylor & Francis, London, 1981.
16. Mangalick, M. E. and Fiore, N. F., *Trans. metall. Soc. A.I.M.E.*, 1968, **242**, 2363.
17. Kröner, E., *Z. Physik*, 1958, **5**, 504.
18. Honeycombe, R. W. K., *Plastic Deformation of Metals*. Cambridge University Press, Cambridge, 1964.
19. Hill, R., *J. Mech. Phys. Solids*, 1965, **13**, 89.
20. Hill, R., *J. Mech. Phys. Solids*, 1967, **15**, 79.
21. Hutchinson, J. W., *Proc. R. Soc. A*, 1970, **319**, 247.
22. Weng, G. J., *Int. J. Plasticity*, 1987, **3**, 315.
23. Hosford, W. F., *The Mechanics of Crystals and Textured Polycrystals*. Oxford University Press, New York, 1993.
24. Tome, C. N., Private communication.